AN OVERVIEW OF GEORGIA TECH STUDIES ON THE FLUID DYNAMICS ASPECTS OF LIQUID PROTECTION SCHEMES FOR FUSION REACTORS

S. I. Abdel-Khalik and M. Yoda

G. W. Woodruff School of Mechanical Engineering, Georgia Institute of Technology, Atlanta, GA 30332–0405 USA
said.abdelkhalik@me.gatech.edu; minami.yoda@me.gatech.edu

This paper provides an overview of experimental and numerical studies conducted at Georgia Tech to assess the fluid dynamics aspects of liquid protection schemes for fusion energy reactors. The problems described here include: (1) Dynamics of slab jets for thick liquid protection, including the effect of nozzle design, flow conditioning, and boundary layer cutting on jet surface smoothness; (2) Primary turbulent breakup of turbulent liquid sheets and forced thin liquid films, and quantification of the associated hydrodynamic source term; (3) Dynamics of forced films on downward-facing flat and curved surfaces, including film detachment and flow around beam ports; (4) Free-surface topology and drop detachment from downward-facing porous wetted walls; and (5) Thermocapillary effects and associated design constraints for liquid-film-protected divertors and first walls.

The experimental data and validated numerical models developed in these studies allow reactor designers to identify design windows for successful operation of liquid-protected first walls and plasma facing components in inertial and magnetic confinement systems.

I. INTRODUCTION

Over the last six years, the Georgia Tech Fusion Engineering Group has carried out a variety of experimental and numerical studies on the fluid dynamics and heat transfer aspects of liquid-protected fusion energy chambers, first walls, and plasma-facing components. Previous studies focused on both thick and thin liquid protection schemes for IFE reactor chamber first walls as proposed in the HYLIFE-II[1] and Prometheus[2] designs. Recent research has also included studies of liquid-protected plasma-facing components for magnetic fusion energy (MFE) applications. This paper provides an overview of these research activities.

In inertial fusion, the energy released from the exploding fuel pellets consists of energetic neutrons, photons, and charged particles that eventually dissipate their kinetic energies in the walls of the reactor chamber. The results of numerous studies on the thermal-mechanical response of chamber first walls have pointed to the need for a first wall protection scheme to assure wall survival at practical chamber sizes. Several such schemes have been proposed over the last three decades, including the use of a sacrificial wall-attached liquid film or free-standing "curtains" to protect the first wall from damaging radiation and thermal stresses.

The HYLIFE-II conceptual design proposed using "thick liquid protection" consisting of arrays of liquid sheets, or slab jets, for both cooling and first wall protection.[1] The Prometheus study, which investigated "thin liquid protection" schemes for both heavy-ion beam and laser drivers, proposed using a thin film of liquid lead to protect the first walls from photons and charged particles.[2] Two types of thin liquid protection schemes were considered: 1) a "wetted wall," with liquid supplied through a porous wall normal to the surface; and 2) a "forced film," where liquid is injected along the surface at high speeds.

In the interval between successive target explosions, the major design issue for liquid protection is how to establish a robust, stable flow that will provide adequate first wall protection while minimizing interference with target injection and driver beams propagation. We have therefore carried out a wide range of experimental and numerical studies on the stability and smoothness of three "building block" flows for liquid protection schemes: 1) vertical turbulent liquid sheets; 2) thin liquid films on a downward-facing flat surface with injection normal to and through the plate; and 3) turbulent forced films over downward-facing flat and curved surfaces.

Both the ALPS and APEX programs have extensively studied plasma surface interactions for liquid-surface-protected plasma facing components.[3,4] These studies established constraints on the maximum fluid surface temperature to limit liquid evaporation and hence plasma impurities; surface temperature limits ranging from 380°C for lithium to 1630°C for tin have been reported.[5,6] Another important design issue for such thin liquid films is the possibility of film rupture and "dryout" due to thermocapillary forces arising from spatial gradients in the wall and liquid surface temperatures; such gradients arise from the expected variations in the incident radiation and particle fluxes. Numerical studies have been conducted to quantify the maximum allowable surface temperature gradients (*i.e.*, heat flux gradients) for various candidate liquids (lithium, flibe, lithium-lead, tin, and gallium) and operating conditions; experimental studies are underway to validate the numerical results.

The remainder of this paper is organized as follows. Section II describes studies aimed at quantifying the effect of various design parameters on jet smoothness and the hydrodynamic source term for thick liquid protection systems. Section III deals with thin liquid protection systems, including both wetted walls and forced films. Section IV deals with thermocapillary effects in thin-liquid-protected plasma-facing components; concluding remarks are provided in Section V.

II. THICK LIQUID PROTECTION STUDIES

HYLIFE-II uses a lattice of stationary liquid sheets of molten Flibe (Li_2BeF_4) to protect the front and back first walls from the fusion explosion while allowing target injection and driver beam propagation (Fig. 1). An array of oscillating sheets forms a protective pocket to shield the chamber sidewalls and dynamically clear the center.[1]

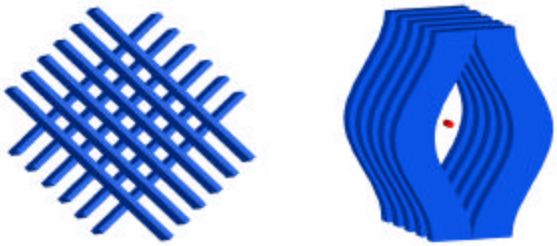

Fig. 1 Lattice of stationary liquid sheets [left] and arrays of oscillating sheets forming a pocket [right].

The fluid mechanics of these flows is characterized by two dimensionless groups: the Reynolds and Weber numbers $Re = U_o ? / ?$ and $We = ? U_o^2 ? / ?$, respectively. Here, U_o is the average speed and ? the jet "thickness" (short dimension) measured at the nozzle exit; ?, ? and ? are the liquid kinematic viscosity, density and surface tension, respectively.

Our group has carried out extensive investigations of various fluid dynamics aspects of this thick liquid protection scheme based on experimental studies of oscillating and stationary turbulent vertical sheets of water issuing into ambient air. Oscillating liquid sheets of a quality sufficient for HYLIFE-II type reactors were demonstrated in the first phase of the studies for (*Re*, *We*) = $(3.7? 10^4, 1.8? 10^3)$.[7]

Surface ripples due to free-surface fluctuations are a major concern in the lattice of stationary sheets since even moderate ripples may interfere with beam propagation and target injection. The free-surface geometry of turbulent liquid sheets has therefore been extensively characterized using planar laser-induced fluorescence (PLIF) in terms of the maximum and standard deviation in free-surface fluctuation as well as a statistically-based liquid cumulative distribution function (LCDF) for various operating conditions and jet nozzle designs for (*Re*, *We*) up to $(1.2? 10^5, 1.9? 10^4)$.[8,9]

The studies demonstrate that a combination of a flow conditioning section and a contracting nozzle produces liquid sheets with surface ripple well within the HYLIFE-II requirements.[9] The flow conditioner (Fig. 2) with an overall *x*-dimension of 21.6 cm consisted of three elements: i) a stainless steel (SS) perforated plate with 4.8 mm diameter staggered holes and 50% open area, ii) 3.8 cm farther downstream, a polycarbonate honeycomb section with 0.32 cm cell diameter and *x*-dimension of 2.5 cm; and iii) 0.5 cm farther downstream, a SS fine screen with 37.1% open area and 0.33 mm wire diameter. The nozzle with an *x*-dimension of 6.3 cm had a 3:1 contraction along its *z*-dimension described by a 5^{th} order polynomial in *x* with a straight inlet and a contraction of 4° at its exit. The nozzle exit dimensions were 10 cm ? ?, where ? = 1 cm. The nozzle inlet was 14.6 cm downstream of the flow straightener; both elements were manufactured using stereolithography rapid prototyping.

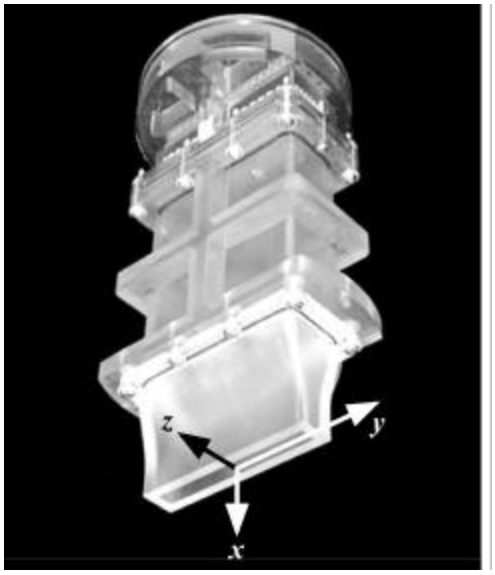

Fig. 2 Flow straightening section and nozzle.

Figure 3 shows two different estimates of surface ripple at (*Re*, *We*) = $(1.2? 10^5, 1.9? 10^4)$ for $x/? ? 25$. Here, $?_z(✍)$ is the standard deviation in the *z*-position of the free surface averaged over $|y| ? 3.75$ cm; $?_3?(✍)$ is the most conservative LCDF-based estimate of the standard deviation averaged over three full standard deviations of the liquid volume fraction ? :

$$?_3?? \frac{z(? \; ? \; 0.0013) ? z(? \; ? \; 0.9987)}{6} \qquad (1)$$

Both surface ripple estimates are below 0.05? for the range of $x/?$ spanning the lattice proposed for HYLIFE-II;

they are also significantly less than the maximum value of 0.07? specified for HYLIFE-II at *Re* and *We* about 50% and 20%, respectively, of prototypical values.[10]

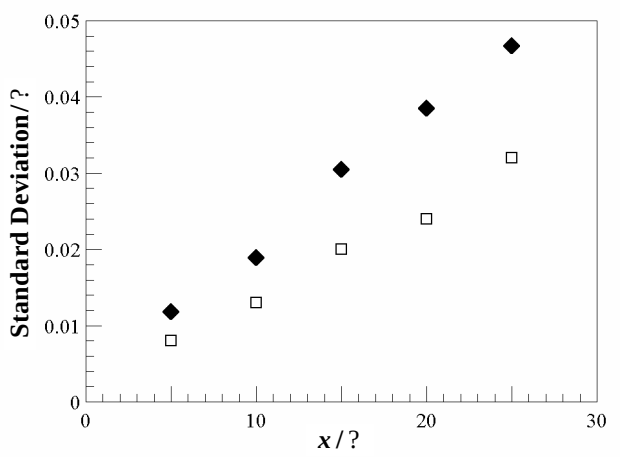

Fig. 3 Normalized surface ripple as a function of normalized downstream distance.

Although several investigators have characterized the dynamics and surface smoothness of liquid sheets and cylindrical jets[11], there have been relatively few studies of the mass ejected from the free surface. This is surprising given that these flows are known to eject drops at *We* far below those required for full atomization.[12] We have therefore quantified the "hydrodynamic source term", *i.e.*, the ejected mass due to turbulent primary breakup, using a simple mass collection technique.[13]

Experimentally based correlations for jets with initial conditions corresponding to fully-developed turbulent pipe flow give the mass flux of drops G ejected from the free surface due to turbulent primary breakup as:

$$G(x) \approx 0.272\,\bar{v}_r \frac{x}{d_h\sqrt{We_d}} \qquad (2)$$

where, $\bar{v}_r \approx 0.04U_o$ is the cross-stream component of the drop velocity measured with respect to the free surface, d_h is the hydraulic diameter of the jet and We_d is the Weber number based upon d_h. The correlation is valid for We_d = 235–270,000.[14]

This breakup is however greatly reduced, and in some cases even eliminated, in round jets if the initial velocity profile is plug (*vs.* turbulent pipe) flow. Our initial measurements showed that Eq. (2) overestimated the actual collected mass flux by at least 3–4 orders of magnitude, probably due to the use of both flow conditioning and a contracting nozzle to create a nearly uniform flow at the nozzle exit.

"Boundary-layer cutting", where a knife edge is used to remove the boundary layer from the flow just upstream of the nozzle exit, has also been shown to greatly reduce the hydrodynamic source term in round jets.[11,15] We have therefore implemented boundary-layer cutting in turbulent liquid sheets.[16] Figure 4 shows the collected mass flow rate converted to number density N as a function of $\Delta z_s/\delta$ for no cutting (✍) and boundary-layer cutting corresponding to removing 1.0% and 1.9% of the total mass flow rate (↴ and ✍, respectively). Here, Δz_s is the distance along z measured from the nozzle inner wall (*cf.* Fig. 2) to the nearest edge of the collector.[13] Given the experimental sensitivity limit shown in the Figure of about 2.1×10^{-19}, these measurements demonstrate that "cutting" as little as 1.9% of the total mass flux essentially eliminates the hydrodynamic source term. Although not shown here, boundary-layer cutting also reduced surface ripple, reducing the standard deviation in the z-position of the free surface by 17%.

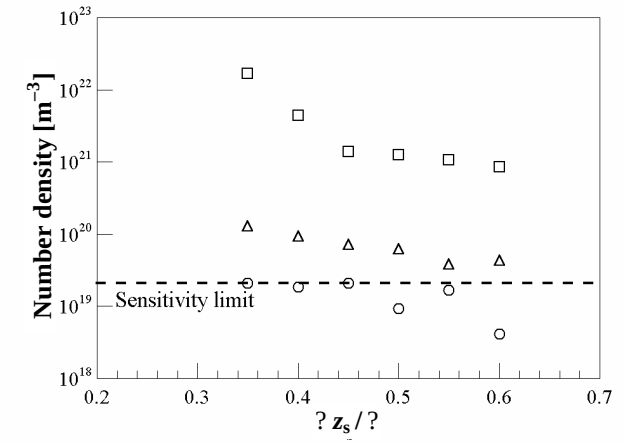

Fig. 4 Hydrodynamic source term in terms of number density as a function of normalized standoff distance.

We are currently using laser-Doppler velocimetry (LDV) to measure profiles of the mean streamwise velocity and rms velocity fluctuations for the x and z velocity components just upstream of the nozzle exit in turbulent liquid sheets.[17, 18] The results of these studies will correlate how these initial conditions, reflecting both nozzle and flow conditioning designs, affect surface ripple and the hydrodynamic source term.

These studies have contributed to our fundamental knowledge of turbulent liquid sheets and expanded the design database available to power plant designers for such flows. Furthermore, this work has demonstrated that high-speed "liquid curtains" can—with appropriate flow conditioning sections, nozzle geometries, and boundary-layer cutting designs—be established that meet current requirements for surface smoothness and stability. Although these results are promising, chamber clearing to remove vapor and drops between fusion events and re-formation of the liquid sheet after the fusion event still remain as major feasibility issues for thick liquid protection schemes.

III. THIN LIQUID PROTECTION

In the Prometheus design, a thin sacrificial film of liquid lead was proposed to shield the first walls of the reactor chamber, an upright cylinder capped with hemispheres at its top and bottom, from X-rays and ions. The film was created using two different methods: 1) a wetted wall, where a 0.5 mm thick layer of liquid lead is supplied through a porous SiC structure; and 2) a forced film, where liquid is injected at speeds exceeding 7 m/s through slots to create a few millimeter-thick attached film over the upper endcap (Fig. 5).[2] Major fluid dynamics issues for thin film liquid protection include preventing film detachment, which may negate the effectiveness of the film as a wall protectant, and preventing drop detachment from the film free-surface which may interfere with target injection and ignition. We have studied the thermal-hydraulic aspects of both types of film flows, focusing on determining general criteria for predicting "worst case" scenarios involving drop formation and film detachment for films on the underside of horizontal and inclined surfaces.

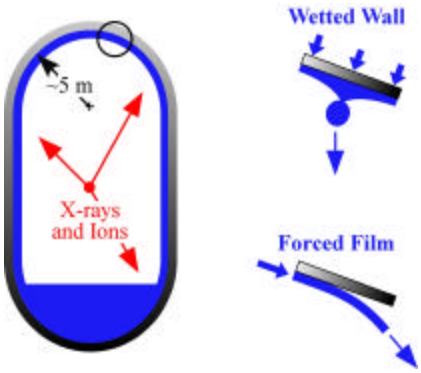

Fig. 5 The Prometheus reactor chamber [left] and the wetted wall and forced film concepts [right].

III.A. Wetted Walls

The model flow for the wetted wall concept is essentially a variation of the classic Rayleigh-Taylor instability where a "heavy" fluid (*i.e.*, molten lead) lies above a lighter fluid (*i.e.*, chamber gas) in a gravitational field pointing downwards with continuous transpiration through and normal to a bounding wall above the heavy fluid. The Georgia Tech group has carried out extensive numerical[19,20] and experimental studies to investigate liquid films on the underside of horizontal and inclined porous walls with injection through the wall. This section briefly reviews recent experimental and numerical studies for validating a numerical code based on a level contour reconstruction front tracking technique.[21] Film thickness and drop detachment times and sizes were measured for different film thicknesses and liquid properties.

In these experiments, water and a mixture of 20% glycerin and 80% (by weight) water were continuously fed from a supply tank and injected through porous sintered stainless steel plates (nominal dimensions 12 cm ? 18 cm). Liquid films on the underside of horizontal and inclined plates at ? = 0? and 2.5? with respect to the horizontal, respectively, were studied. The fluid injection velocity w_{in} and hence mean film thickness z_o (note that w_{in} and z_o are not independent parameters in the experiments) were varied in the recirculating flow facility either by adjusting the height of the tank above the porous plate or varying the plate porosity from 20–45% by volume; the resulting range of injection velocities w_{in} = 0.9–2.1 mm/s.

The important no dimensional parameters for these film flows are the Reynolds and Weber numbers *Re* and *We*; in this case, both are functions only of the fluid properties. Using the Laplace length scale $l = \sqrt{g(\rho - \rho_G)}$ and a velocity scale $U_o = \sqrt{gl}$ (g is the gravitational acceleration and ρ_G is the density of the lighter fluid),[22] $Re = U_o l / \nu$ = 445 and 250 for water and the glycerin-water mixture, respectively, at 293K, which fall within the range of values for candidate liquids (Table I). Given the range of temperatures experienced by any coolant subject to the severe thermal gradients in the reactor chamber, no effort was made to precisely match a *Re* value at a specific temperature. In all cases, the Weber number $We = \rho / (\rho - \rho_G) = 1$.

	Lead		Lithium		Flibe (Li_2BeF_4)		
T (K)	700	800	523	723	773	873	973
Re	1620	1830	1550	1780	82	130	200

Table I Reynolds numbers of various candidate coolants at representative temperatures.

Liquid film thickness was non-intrusively measured using a laser confocal displacement meter (Keyence LT-8110). For ? = 0?, the film thickness was essentially constant over the entire plate surface; the "unperturbed" film thickness was measured at a single location near the center of the plate farthest from departing droplets. For ? = 2.5?, the film thickness varies over the plate, with the greatest thickness at the lowest edge of the plate. Mean film thicknesses were measured at different distances from the upper edge of the plate X = 2, 3, 4 and 5 cm. In all cases, the mean film thickness z_o at a given spatial location increased with w_{in}; z_o values decreased for higher *Re* at a given w_{in}. These experimental data were then used as inputs for the numerical simulations to predict the drop detachment time and detached drop volume.

For the inclined film, the numerical simulations assume a constant film thickness over the entire plate surface since the computational resources required to

simulate the evolution of a film with spatially varying film thickness are prohibitive. Simulations were therefore carried out for a range of constant film thickness values based on the experimentally measured mean film thicknesses at different X with Re = 250 or 445.

Drop formation and detachment were visualized by a CCD camera (Pulnix TM-6710) as 648 ? 484 pixel images at a framing rate of 120 Hz. The images were acquired on a computer HD and processed using a grayscale gradient-based edge detection scheme implemented in MATLAB to measure drop detachment times. In each experimental run, drop detachment occurs at fixed spatial locations (that vary randomly between runs); drop detachment times were therefore measured starting from $?^{exp}$ = 0, or the detachment of the previous drop. The average detachment time t_d^{exp} and the standard deviation $?_t^{exp}$ were then calculated from 100 measurements.

Figure 6 shows a typical drop detachment sequence at Re = 445, ? = 2.5? and w_{in} = 2.1 mm/s. The right panel shows a single 3D numerical simulation result calculated for the same parameters with $?_s / z_o$ = 0.75, where $?_s$ is the initial perturbation amplitude and z_o is the mean film thickness. Unlike the experiments, the simulations are started with an initial perturbation at time $?^{num}$ = 0 since the computational times required to simulate more than one drop detachment are prohibitive. Experimental and numerical "times" are therefore not directly comparable.

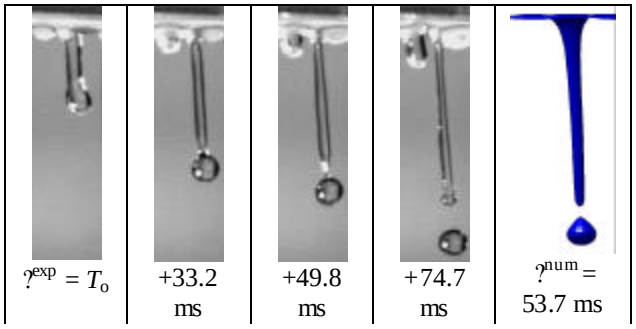

Fig. 6 Drop formation sequence from $?^{exp}$ = 215.8 ms to 290.5 ms [left] and a numerical "snapshot" at t = 269.5 ms [right] at Re = 445, ? = 2.5? and w_{in} = 2.1 mm/s.

In the experiments, drop detachment times and detached drop size both depend strongly on random and uncontrolled perturbations of the film free surface. In the 3D simulations, a sinusoidal perturbation of amplitude $?_s$ is used to start the drop formation and detachment process. Our inability to characterize "initial" perturbations in the experiments precludes direct comparison of experimental and numerical results on drop evolution and detachment. Numerical simulations were therefore carried out for each pair of (z_o, w_{in}) values obtained from the experimental measurements at several different perturbation levels characterized by $?_s$.

Figure 7 shows numerical predictions of normalized drop detachment time $t_d U_o / l$ obtained at different perturbation levels $?_s / z_o$ (✍) at Re = 445, ? = 0? and w_{in} = 0.9 mm/s (black) and 2.1 mm/s (gray). The Figure shows t_d^{exp} as a horizontal solid line; the t_d^{exp} ? 2? $_t^{exp}$ levels are indicated as horizontal dashed lines above and below the solid line. Here, t_d^{exp} ? 2? $_t^{exp}$ = 465 ? 30 ms and 241 ? 28 ms for w_{in} = 0.9 mm/s and 2.1 mm/s, respectively. In both cases, the mean detachment time obtained from the experiments lies within the range of numerical predictions calculated for 0 < $?_s / z_o$? 1.

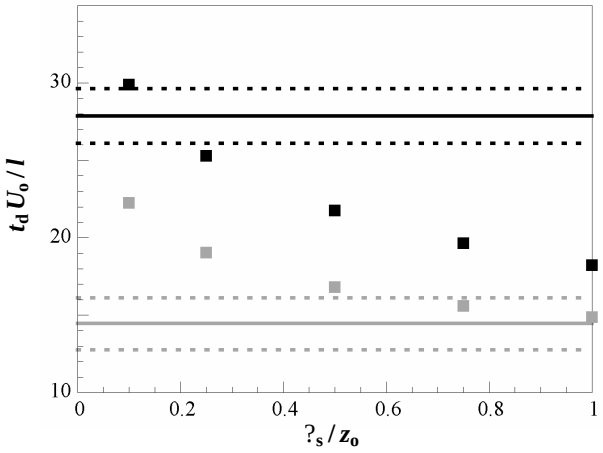

Fig. 7 Detachment time *vs.* perturbation amplitude: Re = 445, ? = 0? and w_{in} = 0.9 (black) and 2.1 mm/s (gray).

Detached drops were approximated as prolate spheroids with semi-major and semi-minor axes a and b, respectively, to calculate the equivalent drop diameter (= $2[ab^2]^{1/3}$). Average equivalent drop diameter D^{exp} and standard deviation $?_D^{exp}$ were calculated from 100 independent experimental samples. Figure 8 shows numerical predictions of normalized equivalent drop diameter D / l (✍) for various values of $?_s / z_o$ at Re = 250 (black) and 445 (gray), ? = 0? and w_{in} = 0.9 mm/s. The values for D^{exp} and D^{exp} ? 2? $_D^{exp}$ are again indicated by solid and dashed horizontal lines, respectively. Here, D^{exp} ? 2? $_D^{exp}$ = 9.0 ? 0.4 mm and 8.2 ? 0.4 mm at Re = 250 and 445, respectively. The Figure shows that D is essentially independent $?_s / z_o$; again, D^{exp} lies within the range of numerical predictions calculated for 0 < $?_s / z_o$? 1 in both cases.

For all Re, w_{in} and ? studied here, t_d^{exp} and D^{exp} were found to lie within the range of numerical predictions obtained for 0 < $?_s / z_o$? 1. In general, t_d^{exp} was in

agreement with numerical simulations at lower values of $?_s / z_o$ for smaller injection velocities and at higher values of $?_s / z_o$ for larger w_{in} (*cf.* Fig. 7). The experimental and numerical results also both show that drop sizes increase with increasing w_{in} and decreasing *Re*, and that D^{exp} tends to be slightly less than the range of numerical predictions for *D*, especially at higher *Re* (*cf.* Fig. 8). These results suggest that the predictions of the numerical simulations can—despite our inability to directly compare numerical simulations and experiments—be used to estimate a minimum repetition rate to avoid liquid dripping into the reactor cavity.

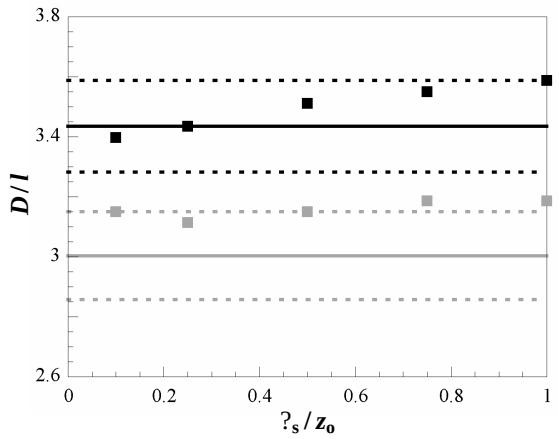

Fig. 8 Equivalent drop diameter *vs.* perturbation amplitude: *Re* = 250 (black) and 445 (gray), ? = 0? and w_{in} = 0.9 mm/s.

III.B Forced Films

Although the Prometheus study envisioned injecting the forced film from a single point at the chamber apex, this is not feasible if the film is completely destroyed by the microexplosion since re-establishment of the film over the entire upper endcap before the next microexplosion would require either very low repetition rates or excessively high liquid velocities. The only feasible implementation of the forced film therefore appears to require "tiling" of the upper endcap with multiple injection and removal slots.

In our studies, turbulent films were experimentally created by tangentially injecting water through rectangular slot nozzles of thickness (short dimension) ? = 1–2 mm onto the underside of downward-facing flat and curved surfaces with a radius of curvature *R* = 5 m. The average detachment length measured from the nozzle exit along the plate surface x_d was determined over four different surfaces with water-solid contact angles ? ? 25°–85° for orientations ? ? 45? below the horizontal at *We* = 100–3200.

Figure 9 shows a typical graph of x_d as a function of *We* for ? = 0? (✍), 30? (↴) and 45? (✍) for ? ? 25° and 85° (open and filled symbols, respectively. At a given *We*, x_d increases as ? increases, corresponding to a decrease in the gravitational component normal to the surface. At a given (*We*, ?), detachment occurs earlier (*i.e.*, x_d decreases) as surface wettability decreases (*i.e.*, ? increases). Although not shown here, the results also demonstrate that surface curvature and associated centrifugal forces stabilizes the film, delaying detachment. The x_d data measured for a flat surface at ? = 0? and ? ? 85° (☞) can therefore be used at a given *We* as a conservative lower estimate of detachment length.

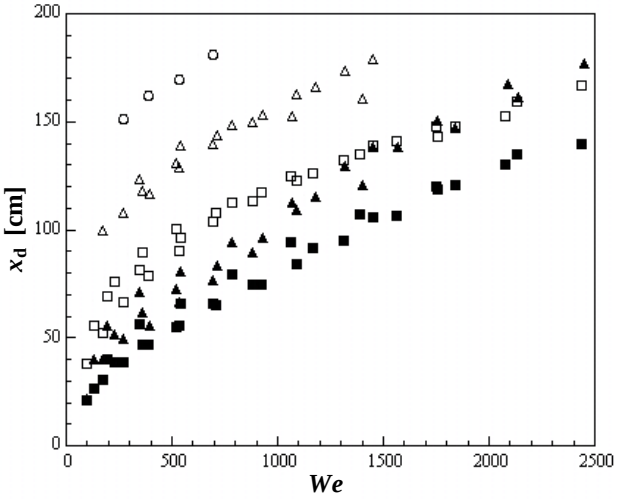

Fig. 9 Detachment length as a function of Weber number.

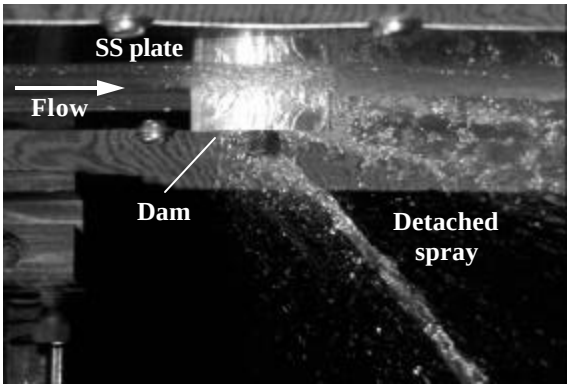

Fig. 10 Detachment of the film around a recessed elliptical dam on a downward-facing flat stainless steel (SS) plate at ? = 0° for *We* = 1000.

The forced-film flow around various types of obstructions modeling the protective dams around beam ports was visualized. Three types of obstructions were studied: cylindrical dams, dams shaped like streamlines for potential flow around a cylinder, and an elliptical dam centered in a conical depression based upon numerical

simulations of hydrodynamically shaped penetrations and backwall modifications carried out by the APEX study.[23] In all cases, the film separated at the obstruction and created a spray of drops falling into the reactor chamber (Fig. 10),[24] suggesting that chamber penetrations may be a significant design challenge for this type of thin liquid protection.

The mass flux of drops ejected from the free surface was also measured for forced films over flat surfaces at ? = 0° for *We* = 1300–2800.[25] Results obtained at distances downstream of the nozzle exit *x*/? = 50–150 imply that even at *We* up to two orders of magnitude below Prometheus values, the collected mass flux *G* can be as great as 5?10^{-3} kg/(m^2?s), or a number density of 2.5?10^{22} m^{-3}; this value is an order of magnitude greater than the background density limit of 3.5?10^{21} m^{-3} given for Prometheus-H corresponding to a chamber pressure limit of 300 mTorr.[2] Furthermore, the experimentally measured number density significantly underestimates the hydrodynamic source term for the prototypical case at *We* up to 1.9?10^5. However, the experiments also suggest that the ejected drops stay near the free surface and hence within the upper endcap of the reactor chamber, with *G* ? 0 (within measurement error) for distances normal to and measured from the mean free-surface position *z* ? 8?. These data suggest that drops ejected from the film free surface due to turbulent primary breakup could preclude placement of driver beams in the upper portion of the reactor chamber for this type of thin liquid protection.

IV. LIQUID-PROTECTED DIVERTORS

Recent work on liquid-surface-protected plasma facing components has resulted in the establishment of operating windows for candidate liquids, as well as limits on the maximum liquid surface temperature in order to limit plasma impurities from liquid evaporation.[3–6] Our work has focused on quantifying the limits, if any, on the maximum allowable surface temperature gradients to assure liquid film stability on liquid-surface- protected plasma facing components; spatial variations in the wall and liquid surface temperatures are expected due to variations in the incident radiation and particle fluxes. Thermocapillary forces created by such temperature gradients can lead to film rupture and dry spot formation in regions of elevated local temperatures.[26] Attention has been initially focused on "non-flowing" thin liquid films similar to those formed on the surface of porous wetted-wall components. Future analysis will include the effects of macroscopic fluid motion and MHD forces.

A numerical model using the level contour reconstruction method[19,26] was used to follow the evolution of the liquid free surface above a non-isothermal surface. Fig. 11 shows typical results for the transient histories of the maximum and minimum film thickness of a thin lithium liquid film with an initially-uniform (2 mm) thickness subjected to a sinusoidally varying surface temperature with different amplitudes.

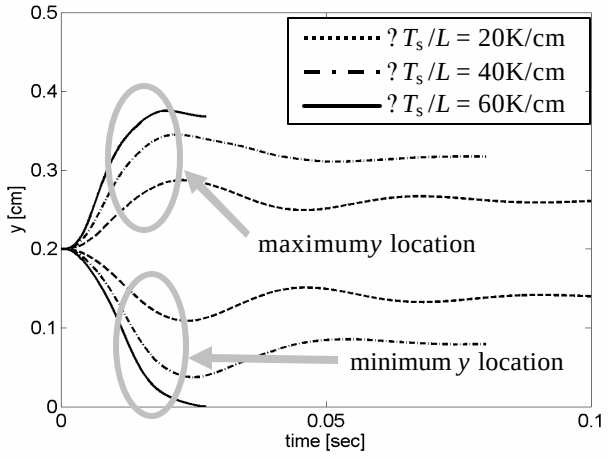

Fig. 11 Transient variations of the maximum and minimum film thickness for a lithium liquid film with initially uniform (2 mm) film thickness subjected to sinusoidal surface temperature variation.

Table II. Maximum temperature gradient limits for different coolants.

Coolant	Mean Temperature [K]	(? T_s / L) [K/cm]	
		Numerical Solution	Asymptotic Solution
Lithium	573	30	13
Li-Lead	673	570	173
Flibe	673	76	38
Tin	1273	113	80
Gallium	1073	600	211

The results show that as the temperature gradient increases the minimum film thickness eventually reaches zero, thereby signifying film rupture. A generalized chart for the maximum non-dimensional temperature gradient as a function of the governing non-dimensional variables, namely, the Weber, Froude, and Prandtl numbers, and aspect ratio, was developed; the chart allows the maximum allowable temperature gradient for a given liquid material, mean temperature, and film thickness to be determined[26]. An asymptotic solution to the governing equations, applicable for low aspect ratios (*i.e.*, thin liquid films) was also developed; the model provides a conservative lower bound for the allowable temperature gradient. Both the numerical model and the asymptotic solution were used to determine the maximum temperature gradients for various candidate liquids, namely lithium, lithium-lead, flibe, tin, and gallium; the results are shown in Table II. These results show that the allowable temperature gradients differ significantly

among the various liquids, and that, in some cases, such constraint may be highly restrictive.

V. CONCLUDING REMARKS

This paper reviews several studies conducted at Georgia Tech on the fluid dynamic of liquid protection schemes for fusion energy reactors. Two types of flows are studied, namely liquid sheets proposed for thick liquid protection of reactor chamber first walls and wall-attached liquid films proposed for thin liquid protection of first walls and plasma-facing components in MFE reactors. Experiments on turbulent liquid sheets involve studies of the effects of initial conditions such as various nozzle geometries, flow conditioning designs, and boundary-layer cutting on free surface smoothness and primary turbulent breakup. Investigations of forced thin liquid films on the underside of flat and curved surfaces focus on their detachment and turbulent primary breakup, as well as the dynamics of such flows in the vicinity of beam ports. Numerical and experimental studies of thin liquid films attached to the underside of porous wetted walls with evaporation and condensation at the free surface have characterized their free- surface topology, including drop detachment times and equivalent diameters. Recent simulations of thermocapillary-induced "dryout" of a thin liquid film above a non-isothermal wall are used to suggest limits for spatial temperature gradients for various candidate coolants.

The experimental data and numerical models developed in these studies allow reactor designers to identify design windows for successful operation of liquid-protected walls and plasma facing components in IFE and MFE systems.

ACKNOWLEDGMENTS

This research would not have been possible without the contributions of the other members of the Georgia Tech fusion engineering group over the last six years: F. Abdelall, J. Anderson, J. Collins, S. Durbin, L. Elwell, T. Koehler, J. Reperant, D. Sadowski, B. Shellabarger and S. Shin. We wish to thank the ARIES team for their suggestions and the U.S. DOE Office of Fusion Energy Sciences for their support of this work through contracts DE-FG02-98ER54499 and DE-FG02-01ER54656.

REFERENCES

[1] R. W. MOIR, ET AL., "HYLIFE-II: A Molten-Salt Inertial Fusion Energy Power Plant Design—Final Report," *Fusion Technol.*, **25**, 5 (1994).

[2] L.M. WAGANER, ET AL., "Inertial Fusion Energy Reactor Design Studies," McDonnell Douglas Report DOE/ER-4101, MDC 92E0008, Volume III (1992).

[3] R.F. MATTAS, "Potential for Advanced Limiter/Divertor Systems," *J. Fusion Energ.*, **17**, 251 (1998).

[4] M.A. ABDOU, ET AL., "On the Exploration of Innovative Concepts for Fusion Chamber Technology," *Fusion Eng. Des.*, **54**, 181 (2001).

[5] R. E. NYGREN, ET AL., "A Fusion Reactor Design with a Liquid First Wall and Divertor," to appear in *Fusion Eng. Des.*, (2004).

[6] T. D. ROGNLIEN and M. E. RENSINK, "Interactions Between Liquid-Wall Vapor and Edge Plasmas," *J. Nucl. Mater.*, **290-293**, 312 (2001).

[7] L.C. ELWELL, D.L. SADOWSKI, M. YODA and S.I. ABDEL-KHALIK, "Dynamics of Oscillating Turbulent Liquid Sheets," *Fusion Technol.*, **39**, 716 (2001).

[8] J.J.R. REPERANT., S.G. DURBIN, M. YODA, S.I. ABDEL-KHALIK, and D.L. SADOWSKI, "Studies of Turbulent Liquid Sheets for Protecting IFE Reactor Chamber First Walls," *Fusion Eng. Des*, **63–64**, 627 (2002).

[9] S.G. DURBIN, T.P. KOEHLER, J.J.R. REPERANT, M. YODA, S.I. ABDEL-KHALIK and D.L. SADOWSKI, "Surface Fluctuation Analysis for Turbulent Liquid Sheets," *Fusion Sci. Technol.*, **45**, 1 (2004).

[10] J.F. LATKOWSKI and W.R. MEIER, "Heavy-Ion Fusion Final Focus Magnet Shielding Design," *Fusion Technol.*, **39**, 798 (2001).

[11] S.J. PEMBERTON, R.P. ABBOTT and P.F. PETERSON, "Thick-Liquid Blanket Configuration and Response for the HIF Point Design," *Fusion Sci. Technol.*, **44**, 294 (2003).

[12] S.P. LIN and R.D. REITZ, "Drop and Spray Formation from a Liquid Jet," *Ann. Rev. Fluid Mech.*, **30**, 85 (1998).

[13] S.G. DURBIN, M. YODA, S.I. ABDEL-KHALIK, D.L. SADOWSKI and T.P. KOEHLER, "Assessment and Control of Primary Turbulent Breakup of Thick Liquid Sheets in IFE Reactor Cavities—'The Hydrodynamic Source Term'," to appear in *Fusion Sci. Technol.* (2005).

[14] SALLAM, K.A., DAI, Z. and FAETH, G.M., "Liquid Breakup at the Surface of Turbulent Round Liquid Jets in Still Gases," *Int. J. Multiphas. Flow*, **28**, 427 (2002).

[15] WU, P.K., MIRANDA, R.F. and FAETH, G.M., "Effects of Initial Flow Conditions on Primary Breakup of Nonturbulent and Turbulent Round Liquid Jets," *Atomization Spray.*, **5**, 175 (1995).

[16] S.G. DURBIN, M. YODA and S.I. ABDEL-KHALIK, "Impact of Boundary-Layer Cutting on Free-Surface Behavior in Turbulent Liquid Sheets," Proceedings of TOFE-16 Conference (2004).

[17] S.G. DURBIN, M. YODA, S.I. ABDEL-KHALIK and D.L. SADOWSKI, "Turbulent Liquid Sheets for Protecting IFE Reactor Chamber First Walls," *Fusion Sci. Technol.*, **44**, 307 (2003).

[18] S.G. DURBIN, M. YODA and S.I. ABDEL-KHALIK, "Flow Conditioning Design in Thick Liquid Protection," submitted to *Fusion Technol.* (2004)

[19] S. SHIN, D. JURIC and S.I. ABDEL-KHALIK, "Hydrodynamic stability of the porous wetted wall protection schemes in IFE reactors," *Fusion Eng. Des.*, **65**, 611 (2003).

[20] M. YODA and S.I. ABDEL-KHALIK, "An Investigation of Fluid Dynamics Aspects of Thin Liquid Film Protection Schemes for IFE Reactor Chambers," to appear in *Fusion Sci. Tech.* (2004).

[21] F.F. ABDELALL, "Experimental and Numerical Studies of the Rayleigh-Taylor Instability for Bounded Liquid Films with Injection Through the Boundary," Ph.D. Thesis, Georgia Institute of Technology (2004).

[22] S. SHIN, F. ABDELALL, D. JURIC, S.I. ABDEL-KHALIK and M. YODA, "Fluid Dynamic Aspects of the Porous Wetted Wall Protection Scheme for IFE Reactors," *Fusion Sci. Technol.*, **43**, 366 (2003).

[23] M.A. ABDOU, ET AL., "On the Exploration of Innovative Concepts for Fusion Chamber Technology," *Fusion Eng. Des.*, **54**, 181 (2001).

[24] B.T. SHELLABARGER, "Experimental Studies of High-Speed Liquid Films on Flat and Curved Downward-Facing Surfaces for IFE Applications," M.S. Thesis, Georgia Institute of Technology (2003).

[25] B.T. SHELLABARGER, S.G. DURBIN, M. YODA, S.I. ABDEL-KHALIK and D.L. SADOWSKI, "Turbulent Primary Breakup in Turbulent Liquid Films on Downward-Facing Surfaces," to appear in *Fusion Sci. Tech.* (2004).

[26] S. SHIN, S. I. ABDEL-KHALIK, M. YODA, and the ARIES Team, "Design Constraints for Liquid-Protected Divertors," Proceedings of TOFE-16 Conference (2004).